Plasma-based polarizer and waveplate at large laser intensity

G. Lehmann and K. H. Spatschek
Institut für Theoretische Physik I, Heinrich-Heine-Universität Düsseldorf, D-40225 Düsseldorf, Germany

(Received 18 February 2018; published 1 June 2018)

A plasma photonic crystal consists of a plasma density grating which is created in underdense plasma by counterpropagating laser beams. When a high-power laser pulse impinges the crystal, it might be reflected or transmitted. So far only one type of pulse polarization, namely the so-called *s* wave (or TE mode) was investigated (when the electric field vector is perpendicular to the plane of incidence). Here, when investigating also so-called *p* waves (or TM modes, where the magnetic field vector is perpendicular to the plane of incidence), it is detected that the transmission and reflection properties of the plasma photonic crystal depend on polarization. A simple analytic model of the crystal allows one to make precise predictions. The first conclusion is that in some operational regime the crystal can act as a plasma polarizer for high-intensity laser pulses. Also, differences in phase velocities for grazing incidence between *s* and *p* polarization are found. Thus, secondly, the crystal can be utilized as a waveplate, e.g., transforming linearly polarized laser light into circular polarization. All these processes extend to laser intensities beyond the damage intensities of so far used solid state devices.

DOI: 10.1103/PhysRevE.97.063201

I. INTRODUCTION

Materials pose a particular challenge for future large-scale, low-intensity photonic integrated circuits [1]. They become even more demanding for high-intensity laser systems [2]. In standard femtosecond laser systems the solid state components are subject to optical damage above fluences on the order of 4 J/cm^2 [3,4]. Providing adequate components is an important issue for achieving highest intensities at reasonable cost [5,6].

Plasma emerges as an attractive medium for light manipulation at high intensities. Novel concepts for laser pulse amplification [7–10] make use of energy transfer from a long and energetic pump laser pulse into a short seed pulse via parametric plasma processes. Both backscattering off a Langmuir wave (Raman scattering) or an ion wave (Brillouin scattering) [11,12] have been investigated [13–19]. Plasma mirrors allow the enhancement of pulse contrast [20]. Furthermore, plasma may be used for information storage and retrieval [21], as strongly dispersive elements [22–25], as optical modulators [26], for cross beam energy transfer [27], and as a diagnostic tool for ultrahigh intensity laser plasma interactions [28]. In inertial confinement fusion experiments, self-generated plasma optics gratings appear [29,30]. Laser redirection by cross-beam power transfer is an important example of a nonlinear optics process which uses laser-plasma instabilities to one's advantage [31].

The present paper deals with the manipulation of the polarization of high-power laser light due to optically structured plasma. Michel *et al.* [32] showed theoretically that optical wave mixing in a plasma can allow for a full control of the polarization state of a probe laser. The refractive index perturbation was derived on the basis of a full kinetic plasma model. The typical pump laser intensity was 10^{15} W/cm^2, while the probe laser had much lower intensity. Ideas for photonics devices such as laser-plasma polarizers and waveplates were presented. An experimental demonstration of the plasma waveplate based on laser-induced birefringence was published recently by Turnbull *et al.* [33]. Another system consisting of a pump and a probe laser beam was investigated by Stark *et al.* [34] in the relativistic regime. Particle-in-cell simulations showed that a relativistic pump creates a relativistically hot anisotropic electron plasma which then can act for the probe as a polarizer or a waveplate to alter the pulse polarization. Changes of the refractive index seen by a probe beam have recently been measured by Turnbull *et al.* [35]. In all cases the intensity of the manipulated light is limited by the requirement that it should be much smaller than the pump.

Substantial plasma density modulations appear in Brillouin-type plasma-based amplification scenarios [12,36]. Within the nonlinear regime of counterpropagating large amplitude laser beams, a structured plasma (grating) can be produced in the form of a plasma photonic crystal. The grating is time dependent (transient); however, it exists long enough to change the properties of a third probe pulse. The capability to act as frequency filter or mirror for high-intensity laser pulses was demonstrated recently [37,38]. Here we will show that the transient plasma photonic crystal may also act as a polarizer and waveplate for short (broadband) laser pulses at high intensities. Important for the present understanding and possible application of the transient plasma photonic crystal will be the possibility to predict its behavior by a simple model. It will be shown that the plasma grating can be modeled by periodic stepwise density distributions. The model will predict a sensitive dependence, e.g., on the height of the largest density peak. In some cases it predicts band gaps for one type of polarization. In any case, the predicted birefringent behavior of the plasma photonic crystal will be compared to particle-in-cell (PIC) simulations. Since, based on this model, band structures can be simply predicted in dependence on various parameters, it will become possible to discover the various potential applications. And indeed, two important applications, namely the applicability as polarizer and waveplate,

respectively, were detected and verified by extensive numerical simulations.

To demonstrate and explain these findings, the manuscript is organized as follows. In the next section we briefly review the production and geometry of a plasma photonic crystal itself. Based on these preliminary notes, in Sec. III we present a simple model and its validation. The predictions for polarization-dependent oblique propagation through the plasma photonic crystal, presented in Sec. IV, is the central physical finding. This will be verified in the following Sec. V by numerical simulations. Section V proposes an operational regime for the plasma photonic crystal as a polarizer and, for another parameter regime, the applicability as a waveplate. The paper is concluded by a short summary and discussion.

II. PLASMA CRYSTAL: SIMPLIFIED MODEL AND ITS VALIDATION

A. Production and geometry of a TPPC

Photonic crystals are systems in which the dielectric function is periodically modulated with a period of the order of an optical wavelength. The modulation gives rise to optical band gaps. The latter are similar to electronic band gaps in solids with discrete atomic lattices [39]. The transient plasma photonic crystal (TPPC) considered here arranges itself self-consistently in the presence of two oppositely propagating (and interacting) laser beams with frequency ω_0. The emerging grating is transient on the time scale of a few picoseconds. Nevertheless, it can be used to manipulate short (probe) laser pulses (of a few femtoseconds duration) with μm wavelengths. The intensity of the probe pulse may be large (e.g., 10^{17} W/cm^2).

The principal idea for a TPPC was published in Refs. [37,38]. When one starts with two counterpropagating, linearly polarized laser beams, a standing wave may be formed. The ponderomotive force first pushes the electrons and leads to the formation of an electrostatic field. The ions react delayed in time. Eventually, the ions drive a ballistic evolution of the plasma density. As soon as the laser beat vanishes, also the electric field almost vanishes and electron and ion densities are almost equal. The electrons remain to be trapped at the nodes of the ponderomotive potential and the fastest countermoving ions start to cross trajectories.

In Fig. 1, the shaded region reproduces the density grating of a typical one-dimensional (1D) crystal (see, e.g., Fig. 3 of Ref. [38]) when only the first four Fourier coefficients are used. The figure shows the density variation in x direction with neighboring peaks separated at the distances of about $\lambda_0/2$, where λ_0 is the laser wavelength. The original density distribution n_0 was constant and well below the critical density n_c; in the case under consideration $n_0 = 0.3n_c$. The critical density n_c is defined through the condition $\omega_0 = \omega_{p0}$, where $\omega_{p0} = \sqrt{4\pi n_0 e^2/m_e}$ is the electron plasma frequency and ω_0 is the laser frequency. The system is homogeneous in y and z direction.

B. Two-stage model and its validation

Next, we construct a simple model for the TPPC. Figure 1 guides us to dump down the density to an ideal grating as

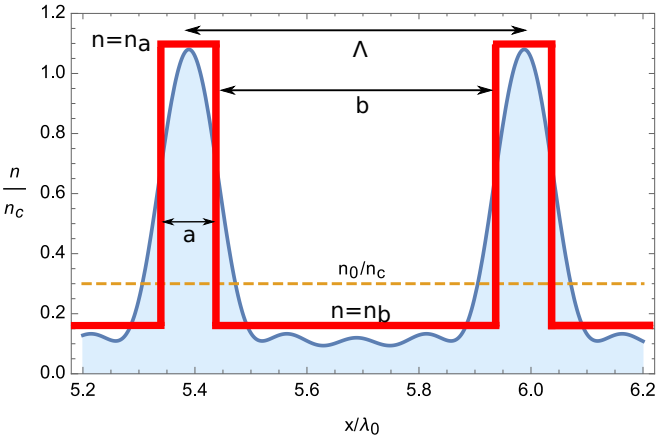

FIG. 1. Outline of a simple model for the density distribution in a crystal which is approximated by a stepwise density variation along the x axis. The broken line shows the original density.

shown in Figs. 1 and 2(a). On the basis of such a simplification we can easily fathom the potential of the TPPC for various applications. For example, we will investigate the behavior of the TPPC for different incident angles θ of laser light, as outlined in the scheme of Fig. 2(c).

However, before presenting any predictions by the model we first should substantiate the general procedure. To validate the ansatz we take over parameter values from previous numerical simulations and compare the predictions of band structure by the simple model (see Fig. 2) with the numerical simulations presented in Refs. [37,38]. When considering a unit cell length $\Lambda = a + b$, where a and b denote the areas of high (n_a) and low density (n_b), respectively, Fig. 1 suggests

$$n_a = 1.1n_c, \quad n_b = 0.1736n_c,$$
$$a = 0.13644\Lambda, \quad b = 0.86356\Lambda. \tag{1}$$

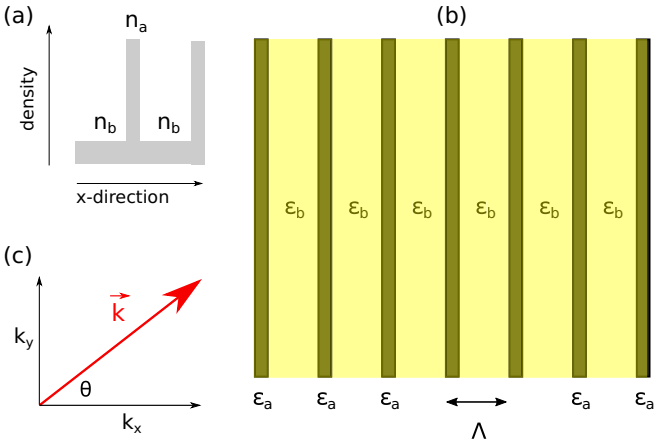

FIG. 2. Outline of a simple model for a TPPC. (a) Stepwise density variation along x axis; (b) top view of the TPPC with unit cell length Λ and variations of the dielectric constant ϵ; (c) geometry of laser light propagation with respect to the arrangement of the crystal (defining the angle of incidence θ).

These values satisfy the normalization condition

$$\frac{an_a + bn_b}{\Lambda} = n_0. \tag{2}$$

As has been discussed in Refs. [37,38], the base length Λ is $\Lambda = \pi/k_1$, where k_1 is the wave number in plasma for a wave entering from vacuum with frequency ω_0 and wave number k_0. Since $k_1 = k_0\sqrt{1-\frac{n_0}{n_c}}$, we have

$$\Lambda = \frac{\lambda_0}{2}\frac{1}{\sqrt{1-\frac{n_0}{n_c}}}. \tag{3}$$

For $\frac{n_0}{n_c} = 0.3$ we obtain $\Lambda = 0.6\,\lambda_0$. We measure frequencies in $2\pi c/\Lambda$. Then the mean electron plasma frequency becomes

$$\Omega_{p0} = \frac{\omega_{p0}\Lambda}{2\pi c} = 0.6\frac{\omega_{p0}}{\omega_0} = 0.6\sqrt{\frac{n_0}{n_c}} \approx 0.3286, \tag{4}$$

while the local plasma frequencies are

$$\Omega_{pb} = \frac{\omega_{pb}\Lambda}{2\pi c} \approx 0.25, \quad \Omega_{pa} = \frac{\omega_{pa}\Lambda}{2\pi c} \approx 0.63. \tag{5}$$

The latter are calculated with densities n_b and n_a, respectively. Wave numbers k will be normalized either by $2\pi/\Lambda$ or by k_1; both normalizations are simply related via

$$K \equiv \frac{k\Lambda}{2\pi} = \frac{1}{2}\frac{k}{k_1}. \tag{6}$$

In a similar way we obtain the relationship

$$\Omega \equiv \frac{\omega\Lambda}{2\pi c} = \frac{\Lambda}{\lambda_0}\frac{\omega}{\omega_0}. \tag{7}$$

Within the layers we specify the dielectric functions

$$\epsilon_a = 1 - \frac{\omega_{pa}^2}{\omega^2} = 1 - \frac{\Omega_{pa}^2}{\Omega^2}, \quad \epsilon_b = 1 - \frac{\omega_{pb}^2}{\omega^2} = 1 - \frac{\Omega_{pb}^2}{\Omega^2}, \tag{8}$$

for a wave with frequency ω approaching the crystal.

We distinguish between two polarization directions of the incoming wave. The s wave is known also as the TE wave because the electric field vector $\vec{E} = E\hat{z}$ is perpendicular to the plane of incidence. Maxwell's equations lead to

$$\left(\frac{\partial^2}{\partial x^2} + \frac{\partial^2}{\partial y^2}\right)E + \epsilon\frac{\omega^2}{c^2}E = 0. \tag{9}$$

For the solutions we impose continuity of E_y and H_z at the interfaces.

The p wave is known also as the TM wave because the magnetic field vector $\vec{H} = H\hat{z}$ is perpendicular to the plane of incidence. Maxwell's equations lead to

$$\frac{\partial}{\partial x}\left(\frac{1}{\epsilon}\frac{\partial H}{\partial x}\right) + \frac{\partial}{\partial y}\left(\frac{1}{\epsilon}\frac{\partial H}{\partial y}\right) + \frac{\omega^2}{c^2}H = 0. \tag{10}$$

For the solutions we impose continuity of E_z and H_y at the interfaces.

The problem of the reflection and transmission of electromagnetic radiation through a multilayer array can be analyzed by the matrix method. We follow the procedure outlined in Ref. [40] and apply the geometry depicted in Fig. 2.

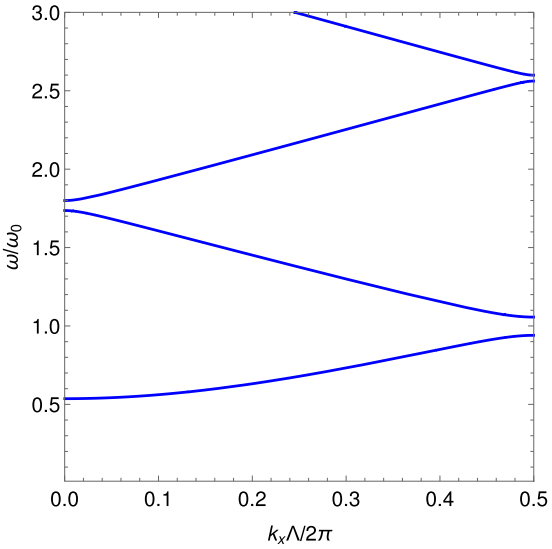

FIG. 3. Model calculation based on the dispersion relations (11) and (13) for propagation with $k_y = 0$. TE and TM modes lead to the same result. It exactly agrees with Fig. 6(a) of Ref. [38].

For TE modes (s polarization) the band structure of the periodic layered medium follows from the dispersion relation

$$\cos(2\pi K_x) = \cos\left(2\pi\frac{a}{\Lambda}K_{xa}\right)\cos\left(2\pi\frac{b}{\Lambda}K_{xb}\right) - \frac{1}{2}\left(\frac{K_{xa}}{K_{xb}} + \frac{K_{xb}}{K_{xa}}\right)\sin\left(2\pi\frac{a}{\Lambda}K_{xa}\right) \times \sin\left(2\pi\frac{b}{\Lambda}K_{xb}\right), \tag{11}$$

where

$$K_{xa} = \sqrt{\Omega^2 - \Omega_{pa}^2 - K_y^2}, \quad K_{xb} = \sqrt{\Omega^2 - \Omega_{pb}^2 - K_y^2}. \tag{12}$$

Equation (11) is a relation between normalized frequency $\Omega = \frac{\omega\Lambda}{2\pi c}$ and wave vector components $K_x = \frac{k_x\Lambda}{2\pi}$ and $K_y = \frac{k_y\Lambda}{2\pi}$.

For TM modes (p polarization) we obtain the slightly different dispersion relation

$$\cos(2\pi K_x) = \cos\left(2\pi\frac{a}{\Lambda}K_{xa}\right)\cos\left(2\pi\frac{b}{\Lambda}K_{xb}\right) - \frac{1}{2}\left(\frac{K_{xa}}{K_{xb}}\frac{\Omega^2 - \Omega_{pb}^2}{\Omega^2 - \Omega_{pa}^2} + \frac{K_{xb}}{K_{xa}}\frac{\Omega^2 - \Omega_{pa}^2}{\Omega^2 - \Omega_{pb}^2}\right) \times \sin\left(2\pi\frac{a}{\Lambda}K_{xa}\right)\sin\left(2\pi\frac{b}{\Lambda}K_{xb}\right). \tag{13}$$

One recognizes immediately that for $K_y = 0$, i.e., for normal incidence onto the array, the two dispersion relations (11) and (13) are identical. They can be easily solved, e.g., with MATHEMATICA. The result is shown in Fig. 3 for $K_y = 0$. We have drawn $\frac{\omega}{\omega_0}$ versus K_x to directly compare with Fig. 6(a) of [38]. The agreement between the present model (stepwise layered material) with the numerical findings is excellent. Only modes with $\omega/\omega_0 > \sqrt{n_0/n_c}$ will propagate.

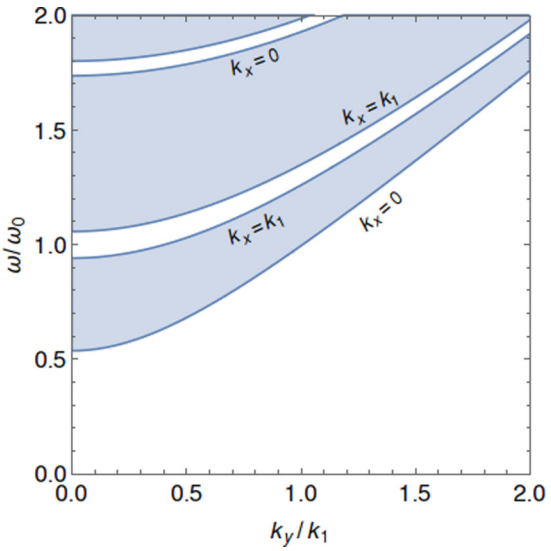

FIG. 4. Band structure for oblique propagation ($k_y \neq 0$) of TE modes, as calculated from the dispersion relation (11). For the TE modes we obtain exact agreement with the previous result of Fig. 8 in Ref. [38].

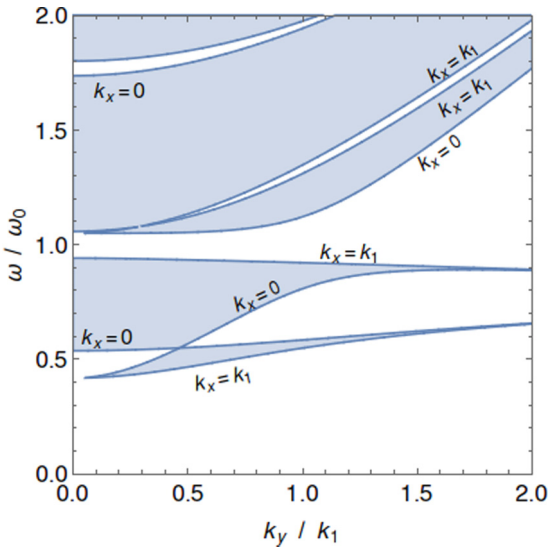

FIG. 5. Band structure for oblique propagation ($k_y \neq 0$) of TM modes, as obtained from the dispersion relation (13).

III. PREDICTIONS FOR POLARIZATION-DEPENDENT OBLIQUE PROPAGATION

A. TE modes

When investigating oblique propagation, we start with TE modes. Again, for this case numerical simulations are already available, for example, those published in Fig. 8 of Ref. [38]. When evaluating the dispersion relation (11) for the parameters (1) we find the band structure shown in Fig. 4. The shaded areas are zones of allowed bands in which $|\cos(2\pi K_x)| < 1$. They exactly agree with the band structure occurring in the numerical simulations [37,38]. Now, the analytic model (11) easily explains the form of the bands.

Since in (11) frequency and transverse wave number only occur in the combination $\Omega^2 - K_y^2$, the analytic model for TE modes obviously predicts the dependence

$$\Omega^2 = \Omega_0^2 + K_y^2, \tag{14}$$

which occurs in Fig. 4. The constants Ω_0 for the boundaries of the bands follow from Fig. 3 (which is for $K_y = 0$) when we set $|\cos(2\pi K_x)| = 1$. In conclusion, the discovery of the dependence (14) in the simulations for the oblique propagation of TE modes provides another successful test of our analytic model.

B. TM modes

The different forms of the dispersion relations (11) and (13) for $K_y \neq 0$ suggest that the oblique propagation becomes polarization dependent (birefringent). And indeed, when analyzing TM waves with (13) for $K_y \neq 0$, the behavior is different. In Fig. 5, we plot the TM band structure for the parameters mentioned in Sec. II B. Several features are interesting. First, we find significant phase-velocity differences between TE and TM modes. Second, there is now a band gap around $\omega = \omega_0$. Considering that frequency range, TM polarized waves will not propagate inside the crystal, irrespective of the incident angle. This feature can be exploited to use the plasma crystal as a polarizer. Third, the dispersion relation predicts propagation of TM polarized light for frequencies $\omega/\omega_0 < \sqrt{n_0/n_c}$. The low frequency cutoff for TM modes is now determined by the density n_b ($<n_0$), i.e., ω/ω_0 only has to be larger than $\sqrt{n_b/n_c}$. For such modes the initially homogeneous plasma appears overdense. However, the lower density stripes in the grating allow for propagation as long as they are underdense.

IV. SIMULATION RESULTS

We conducted two-dimensional (2D) particle-in-cell (PIC) simulations using the EPOCH code [41]. All simulations started from a homogeneous plasma slab of dimension 30 μm $\times$ 45 μm and $n_0 = 0.3n_c$. We assume an electron-proton plasma with ion mass $m_i = 1836m_e$. The choice of the relatively high plasma density $n_0 = 0.3n_c$ facilitates the buildup of dense plasma steps with $n_a > n_c$ at relatively low pump intensities of the lasers which create the crystal. For an optical polarizer we need $n_a > n_c$. The plasma density and/or pump intensity requirements are less restrictive for waveplates which are realized with $n_a, n_b < n_c$. The electron temperature is set to $T_e = 25$ eV, and the ion temperature is lower than the electron temperature, i.e., $T_i = T_e/10$. The reason for the choice of low temperatures is similar to the previous argument, i.e., higher temperatures would require larger driver pulse intensities [38].

A. Plasma optical polarizer

We first treat the case when the plasma slab is illuminated by two 800 nm, 200 fs flat-top laser pulses of intensity 5×10^{15} W/cm^2 propagating in positive and negative x direction, respectively. The beat of the lasers drives a one-dimensional plasma grating that is structured along the x direction and (almost) constant along y. At $t = 750$ fs the density profile along x is close to the profile shown in Fig. 1. For an optical

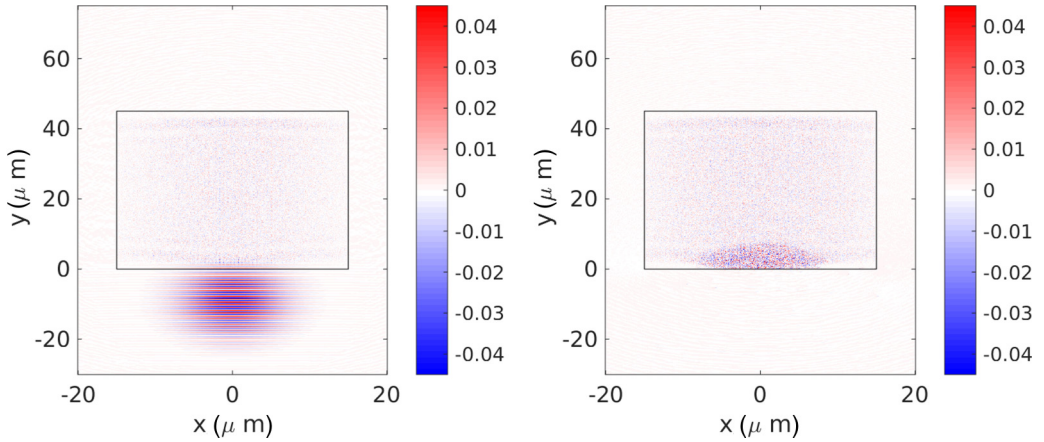

FIG. 6. Electric field E_x corresponding to the TM component of a 50 fs, 800 nm laser pulse that probes a one-dimensional plasma crystal in y direction ($\theta = \pi/2$). The plasma structure is located between $y = 0$ and $y = 45$ μm and is outlined by the box. The fields are shown at times $t = 0.77$ ps (left) and $t = 1$ ps (right), respectively. The grating is opaque for the TM mode.

polarizer we need $n_a > n_c$ and $n_b < n_c$ which are realized with the intensities 5×10^{15} W/cm^2 in an underdense plasma with $n_0 = 0.3n_c$.

To probe the grating, we send a 50 fs (FWHM of electric field), 800 nm (central wavelength) probe pulse of intensity 10^{16} W/cm^2 propagating in positive y direction onto the plasma. The polarization plane of the probe pulse is tilted by 45° with respect to the x, y plane, i.e., it has equal amounts of TE and TM polarization. Figures 6 and 7 show the temporal evolution of the transverse electric fields associated to the two polarization components. The pulse is injected from the boundary at $y = -20$ μm; the plasma grating is located between $y = 0$ and $y = 45$ μm. The electric field is normalized by $m_e c\omega_0/e$. Once the probe pulse interacts with the plasma, we observe that the TE component of the pulse propagates through the grating, while the TM component is blocked. This behavior is in complete agreement with the band structures shown in Figs. 4 and 5. We find that close to 98% of the energy in the TE mode is transmitted. On the other hand, 25% of the total energy in the TM mode is reflected. The other 75% of incident TM energy is absorbed at the surface of the grating. The absorption goes along with a local modification of the electron density at the grating entrance. The discrepancy between the present PIC simulations and the predictions by the two-step model point onto complex kinetic processes near the surface which need further clarification.

In the present case, the plasma grating acts as a polarizer and filters out almost all TM polarized components of a laser pulse. The intensity limit for this filter is determined by the condition that the ponderomotive force of the TE component of the probe laser must not induce significant changes on the electron density profile during its fast propagation through the crystal.

B. Plasma optical waveplate

Plasma gratings in which the maximum electron density is less than the critical density do not show a complete band gap for TM modes. Then, similar to the previously discussed TE case [37,38], TM modes may propagate through the grating when the incidence angle θ is above a critical value. However, the phase velocities of TE and TM modes are different, and the plasma crystal becomes birefringent. Birefringence suggests using the plasma grating as an optical waveplate. To

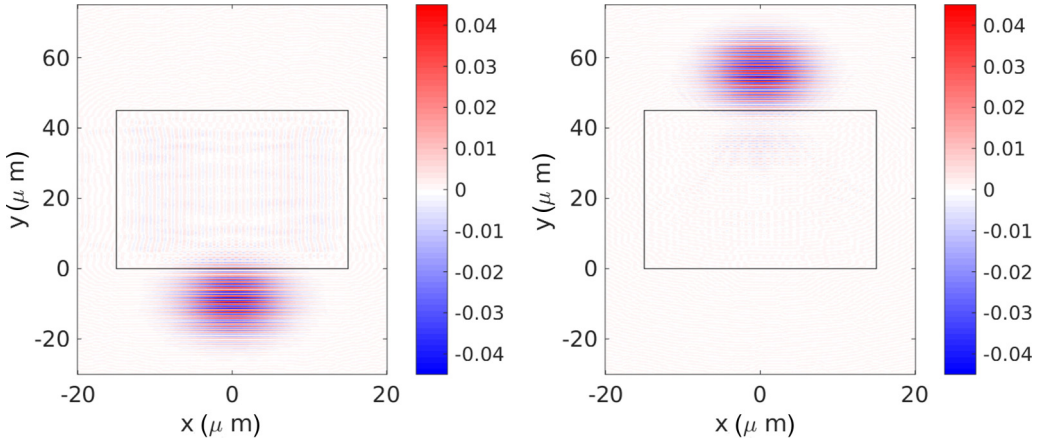

FIG. 7. Electric field E_z corresponding to the TE component of a 50 fs, 800 nm laser pulse that probes a one-dimensional plasma crystal in y direction ($\theta = \pi/2$). Otherwise, the configuration is the same as in Fig. 6. The grating is transparent for the TE mode.

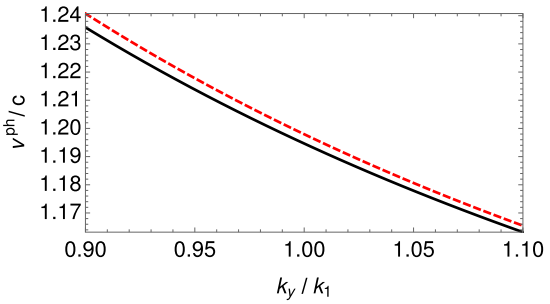

FIG. 8. Phase velocities of waves with TE (black solid) and TM (red dashed) polarization for $k_x = 0$ and the parameters (15).

demonstrate this effect, we conducted PIC simulations with the same initial plasma conditions as before, but reduced the intensity of the laser pulses that drive the grating to $I = 1 \times 10^{15}$ W/cm^2. Then weaker electron density steps with $n_a, n_b < n_c$ appear. In contrast to the values shown in Sec. II B, we may now approximate the resulting density by a stepwise profile with

$$n_a \approx 0.384 n_c, \quad n_b \approx 0.255 n_c,$$
$$a \approx 0.35\Lambda, \quad b \approx 0.65\Lambda. \tag{15}$$

For simplicity, we assume that the incidence angle of the probe pulse is again $\theta = \pi/2$, i.e., $\vec{k} = k_y \hat{y}$. Figure 8 shows the phase velocities $v^{\rm ph} = \omega/k_y$ for waves with frequencies close to ω_0 (i.e., $k_y \approx k_1$) propagating in the positive y direction. The two curves are obtained from the dispersion relations (11) and (13), respectively. We recognize that in this k range the phase velocities are almost linear functions of k. In addition, $v_{TM}^{\rm ph}$ is about 0.28% larger than $v_{TE}^{\rm ph}$ (for $k_y \approx k_1$). The phase velocity difference leads to a phase shift between TE and TM components. The shift accumulates over the propagation distance L. The phase shift in radians, termed retardation Γ, after a distance L is

$$\Gamma = k_1 L \left(\frac{v_{TM}^{\rm ph}}{v_{TE}^{\rm ph}} - 1 \right). \tag{16}$$

Assuming that the probe laser pulse is initially linearly polarized with equal amounts of TM and TE contributions, we can now determine L, which produces a retardation of $\Gamma = \pi/4$. That will change the polarization from linear to circular. In other words, the plasma crystal will behave as a zero-order waveplate. Of course, with extended plasma lengths, phase shifts of $\Gamma = (2n + 1/4)\pi$, $n = 1,2,\ldots$ can be accomplished, corresponding to multiorder waveplates of similar behavior. According to Eq. (16), we expect a (minimum) propagation distance of about 45 μm for a zero-order $\lambda/4$ waveplate.

Figure 9 shows results from a PIC simulation where an initially linear polarized 50 fs probe laser pulse with intensity $I = 10^{16}$ W/cm^2 propagates in positive y direction through the above mentioned grating. On the left-hand side the electric field magnitude of the laser pulse is shown at two different instances in time, before and after passing the plasma. The plasma crystal with its electron density variations is overlayed. On the right-hand side we depict the corresponding transverse electric field amplitude over one wavelength close to the maximum of the respective laser pulse. The polarization undergoes a clear change from linear to circular. The phase difference between the TE and the TM modes of the outgoing pulse is close to $\Gamma = \pi/4$, again showing that the analytic model matches the numerical findings. The total energy transmission is close to 95% of the incident energy.

As the ratio of the phase velocities depends on k_y, the transition from linear to circular polarization can never be perfect for short pulses with a broad bandwidth. The FWHM bandwidth $\Delta\omega/\omega$ of a laser pulse with a FWHM duration (of the electric field) of τ is approximately

$$\frac{\Delta\omega}{\omega} \approx \frac{2.35}{\tau[\text{fs}]}. \tag{17}$$

A 50 fs laser pulse will thus approximately have wave number contributions in the range between $0.95k_1$ and $1.05k_1$. The difference in $v_{TM}^{\rm ph}/v_{TE}^{\rm ph}$ between the central wave number k_1 and the wave numbers $k_1 \pm 0.05k_1$ is around 18%. This is similar to the performance of solid-state zero-order waveplates (for intended polarization changes from linear to circular) in the case of short laser pulses. However, the solid-state devices can only sustain intensities several orders of magnitude less than the plasma gratings. The plasma grating would thus allow one to change the polarization from linear to circular after all beam imaging optics that otherwise do not strictly conserve polarization.

V. SUMMARY AND DISCUSSION

In conclusion, plasma-based optics is a trendsetting technique which may operate at much higher intensities and fluences than what solid materials can withstand. Stimulated Raman and Brillouin processes are known to produce diffractive cells that can manipulate light at high intensities. It was shown recently that a standing pattern produced by counterpropagating laser beams can act as a crystal-like structure (transient plasma photonic crystal). The latter incorporates nonlinear electron and ion dynamics and slow overall time dependence. The present paper demonstrates that a simple model can be developed which covers most of the behavior, although, in principle, the physics of a transient plasma photonic crystal is quite complex. Based on the model, one can make predictions in a broad parameter regime for both TE as well as TM modes, which will guide elaborate numerical simulations for an ultimate verification.

Based on the semianalytic model two applications of the transient photonic plasma crystal were found, namely as polarizer and plasma waveplate, respectively. First, a strongly driven transient photonic plasma crystal with overcritical density peaks shows significantly different band structures for TE and TM modes, respectively. There is a flat band gap for TM modes in the frequency range $\omega \approx \omega_0$. It indicates that TM polarized waves incident on the crystal will not propagate, irrespective of the incident angle. On the other hand, TE modes will go through, almost without any dissipation. This different behavior is the cause for the possible application of a transient plasma photonic crystal as a polarizer. The effect has been verified by numerical simulations.

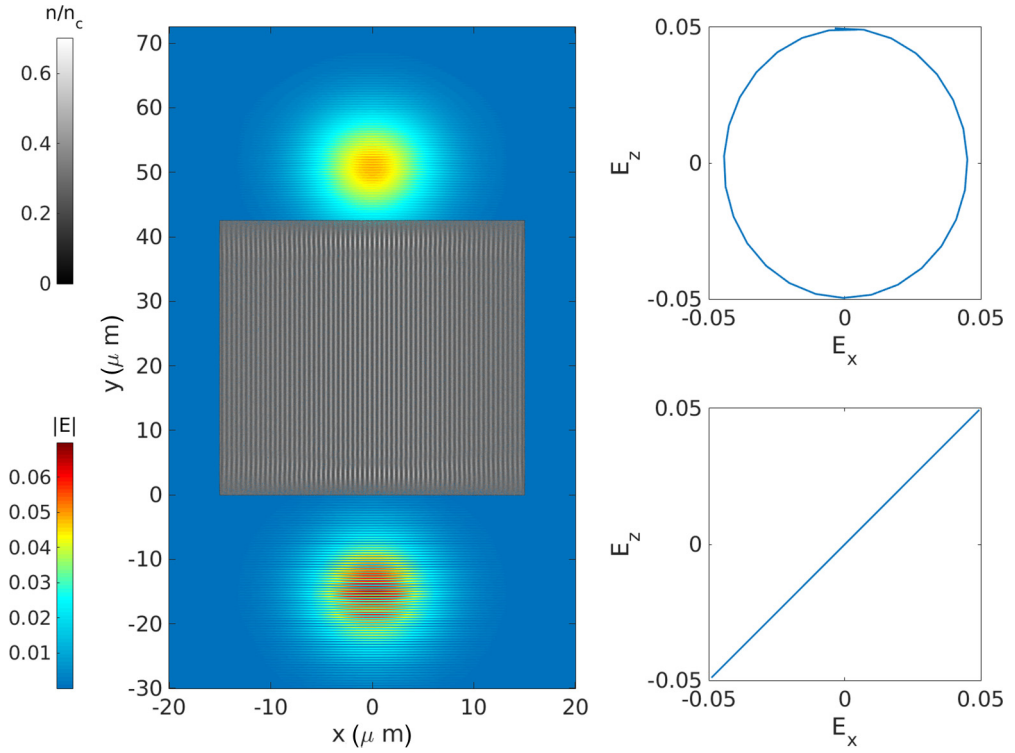

FIG. 9. On the left hand side, the electric field magnitude $|E|$ of an initially linear polarized laser pulse (color) is depicted before and after passing through a plasma grating (gray) with parameters (15). We have $k_x = 0$. On the right we show the transverse electric field amplitude of the laser pulse before (bottom) and after (top) passing through the plasma grating. The amplitude is shown over one wavelength along the y direction, close to the respective pulse maximum.

Secondly, the transient plasma photonic crystal can be utilized to change polarization of a laser pulse. For that case, we created a weakly driven crystal such that the density peaks remain undercritical. The transverse band structure still differentiates between TE and TM modes. It manifests itself in slightly different phase velocities. We verified the predictions of the semianalytic model by PIC simulations. When compared to analogous solid state devices, the key advantage is possible operation at much higher intensities and fluences. With respect to the bandwidth dependency factor for short pulses, at the moment the comparison between plasma and solid-state devices ends in a draw.

ACKNOWLEDGMENTS

The authors gratefully acknowledge discussions with Carsten Müller and Georg Pretzler. The computing time was granted by the John von Neumann Institute for Computing (NIC) and provided on the supercomputers JURECA at Jülich Supercomputing Centre (JSC). Additional computational support and infrastructure was provided by the Centre for Information and Media Technology (ZIM) at the University of Düsseldorf (Germany). Development of the EPOCH PIC code used in this work was in part funded by the UK EPSRC Grants No. EP/G054950/1, No. EP/G056803/1, No. EP/G055165/1, and No. EP/ M022463/1.

[1] D. Dai, J. Bauters, and J. E. Bowers, Light: Sci. Appl. **1**, e1 (2012).
[2] R. K. Kirkwood *et al.*, Nat. Phys. **14**, 80 (2018).
[3] D. Du, X. Liu, G. Korn, J. Squier, and G. Mourou, Appl. Phys. Lett. **64**, 3071 (1994).
[4] A.-C. Tien, S. Backus, H. Kapteyn, M. Murnane, and G. Mourou, Phys. Rev. Lett. **82**, 3883 (1999).
[5] S. Hocquet, J. Néauport, and N. Bonod, EPJ Web Conf. **59**, 07002 (2013).
[6] *Laser-Induced Damage in Optical Materials*, edited by D. Ristau (CRC Press, Boca Raton, FL, 2014).
[7] M. Maier, W. Kaiser, and J. A. Giordmaine, Phys. Rev. Lett. **17**, 1275 (1966).
[8] R. D. Milroy, C. E. Capjack, and C. R. James, Phys. Fluids **22**, 1922 (1979).
[9] S. Suckewer, Nat. Phys. **7**, 11 (2011).
[10] G. A. Mourou *et al.*, Opt. Commun. **285**, 720 (2012).
[11] V. M. Malkin, G. Shvets, and N. J. Fisch, Phys. Rev. Lett. **82**, 4448 (1999).
[12] A. A. Andreev, C. Riconda, V. T. Tikhonchuk, and S. Weber, Phys. Plasmas **13**, 053110 (2006).
[13] G. Shvets, N. J. Fisch, A. Pukhov, and J. Meyer-ter-Vehn, Phys. Rev. Lett. **81**, 4879 (1998).
[14] R. M. G. M. Trines *et al.*, Nat. Phys. **7**, 87 (2011).
[15] G. Lehmann, K. H. Spatschek, and G. Sewell, Phys. Rev. E **87**, 063107 (2013).

[16] J. P. Farmer and A. Pukhov, Phys. Rev. E **92**, 063109 (2015).
[17] G. Lehmann and K. H. Spatschek, Phys. Plasmas **22**, 043105 (2015).
[18] C. Riconda *et al.*, Plasma Phys. Control. Fusion **57**, 014002 (2015).
[19] M. Chiaramello, F. Amiranoff, C. Riconda, and S. Weber, Phys. Rev. Lett. **117**, 235003 (2016).
[20] C. Thaury *et al.*, Nat. Phys. **3**, 424 (2007).
[21] I. Y. Dodin and N. J. Fisch, Phys. Rev. Lett. **88**, 165001 (2002).
[22] Z. Sheng, J. Zhang, and D. Umstadter, Appl. Phys. B **77**, 673 (2003).
[23] H. Wu, Z. Sheng, Q. Zhang, Y. Cang, and J. Zhang, Laser Part. Beams **23**, 417 (2005).
[24] S. Suntsov, D. Abdollahpour, D. G. Papazoglou, and S. Tzortzakis, Appl. Phys. Lett. **94**, 251104 (2009).
[25] M. Durand, Y. Liu, B. Forestier, A. Houard, and A. Mysyrowicz, Appl. Phys. Lett. **98**, 121110 (2011).
[26] L.-L. Yu *et al.*, Nat. Commun. **7**, ncomms11839 (2016).
[27] P. Michel, L. Divol, E. A. Williams, S. Weber, C. A. Thomas, D. A. Callahan, S. W. Haan, J. D. Salmonson, S. Dixit, D. E. Hinkel, M. J. Edwards, B. J. MacGowan, J. D. Lindl, S. H. Glenzer, and L. J. Suter, Phys. Rev. Lett. **102**, 025004 (2009).
[28] S. Monchocé, S. Kahaly, A. Leblanc, L. Videau, P. Combis, F. Réau, D. Garzella, P. D'Oliveira, Ph. Martin, and F. Quéré, Phys. Rev. Lett. **112**, 145008 (2014).
[29] S. H. Glenzer *et al.*, Science **327**, 1228 (2010).
[30] P. Michel, L. Divol, R. P. J. Town, M. D. Rosen, D. A. Callahan, N. B. Meezan, M. B. Schneider, G. A. Kyrala, J. D. Moody, E. L. Dewald, K. Widmann, E. Bond, J. L. Kline, C. A. Thomas, S. Dixit, E. A. Williams, D. E. Hinkel, R. L. Berger, O. L. Landen, M. J. Edwards, B. J. MacGowan, J. D. Lindl, C. Haynam, L. J. Suter, S. H. Glenzer, and E. Moses, Phys. Rev. E **83**, 046409 (2011).
[31] J. D. Moody *et al.*, Nat. Phys. **8**, 344 (2012).
[32] P. Michel, L. Divol, D. Turnbull, and J. D. Moody, Phys. Rev. Lett. **113**, 205001 (2014).
[33] D. Turnbull, P. Michel, T. Chapman, E. Tubman, B. B. Pollock, C. Y. Chen, C. Goyon, J. S. Ross, L. Divol, N. Woolsey, and J. D. Moody, Phys. Rev. Lett. **116**, 205001 (2016).
[34] D. J. Stark, C. Bhattacharjee, A. V. Arefiev, T. Toncian, R. D. Hazeltine, and S. M. Mahajan, Phys. Rev. Lett. **115**, 025002 (2015).
[35] D. Turnbull, C. Goyon, G. E. Kemp, B. B. Pollock, D. Mariscal, L. Divol, J. S. Ross, S. Patankar, J. D. Moody, and P. Michel, Phys. Rev. Lett. **118**, 015001 (2017).
[36] G. Lehmann and K. H. Spatschek, Phys. Plasmas **23**, 023107 (2016).
[37] G. Lehmann and K. H. Spatschek, Phys. Rev. Lett. **116**, 225002 (2016).
[38] G. Lehmann and K. H. Spatschek, Phys. Plasmas **24**, 056701 (2017).
[39] K. Ohtaka, Phys. Rev. B **19**, 5057 (1979).
[40] P. Yeh, *Optical Waves in Layered Media* (Wiley, New York, 1988).
[41] T. D. Arber *et al.*, Plasma Phys. Controlled Fusion **57**, 113001 (2015).